A mixed modality approach towards Xi reactivation for Rett syndrome and other X-linked disorders

Lieselot L. G. Carrette[a,b,c,d], Chen-Yu Wang[a,b,c], Chunyao Wei[a,b,c], William Press[a,b,c], Weiyuan Ma[e,f], Raymond J. Kelleher III[e,f], and Jeannie T. Lee[a,b,c,1]

[a]Howard Hughes Medical Institute, Massachusetts General Hospital, Boston, MA 02114; [b]Department of Molecular Biology, Massachusetts General Hospital, Boston, MA 02114; [c]Department of Genetics, Harvard Medical School, Boston, MA 02115; [d]Center for Medical Genetics, Ghent University, 9000 Ghent, Belgium; [e]Center for Genomic Medicine, Massachusetts General Hospital, Boston, MA 02114; and [f]Department of Neurology, Massachusetts General Hospital, Boston, MA 02114

Contributed by Jeannie T. Lee, December 1, 2017 (sent for review August 28, 2017; reviewed by Ingolf Bach and Gyorgyi Csankovszki)

The X-chromosome harbors hundreds of disease genes whose associated diseases predominantly affect males. However, a subset, including neurodevelopmental disorders, Rett syndrome (RTT), fragile X syndrome, and CDKL5 syndrome, also affects females. These disorders lack disease-specific treatment. Because female cells carry two X chromosomes, an emerging treatment strategy has been to reawaken the healthy allele on the inactive X (Xi). Here, we focus on methyl-CpG binding protein 2 (MECP2) restoration for RTT and combinatorially target factors in the interactome of Xist, the noncoding RNA responsible for X inactivation. We identify a mixed modality approach combining an Xist antisense oligonucleotide and a small-molecule inhibitor of DNA methylation, which, together, achieve 30,000-fold MECP2 up-regulation from the Xi in cultured cells. Combining a brain-specific genetic *Xist* ablation with short-term 5-aza-2′-deoxycytidine (Aza) treatment models the synergy in vivo without evident toxicity. The Xi is selectively reactivated. These experiments provide proof of concept for a mixed modality approach for treating X-linked disorders in females.

X reactivation | antisense oligonucleotides | LNA | Rett syndrome | Xist

Diseases caused by a mutation on the mammalian X chromosome affect males and females differently as males have only one X chromosome and females have two. Female X chromosomes are, however, subject to a dosage compensation mechanism in which one X chromosome is inactivated. Because of "X-chromosome inactivation" (XCI), the female mammal is a mosaic of cells that expresses either the maternal or paternal X chromosome (1–3). Thus, heterozygous X-linked mutations would affect approximately half of a female's somatic cells. For gene products with a non–cell-autonomous function, healthy cells can usually compensate for those expressing the mutation (e.g., factor VIII for hemophilia). With mutations in gene products that fulfill a critical role within the cells that produce them on the other hand, deficits in just half of the body's somatic cells can result in a severe disorder. One well-known example is Rett syndrome (RTT), a human neurodevelopmental disorder caused by a mutation in the methyl-CpG binding protein 2 (MECP2) (4), a chromatin-associated gene product that is crucial for neuronal development. Whereas males do not survive, females are typically born and remain symptom-free until the first or second year of life. Then, symptoms arise that include motor abnormalities, severe seizures, absent speech, and autism (5). To date, no disease-specific therapy is available for this disorder, which affects one in ∼10,000 girls throughout the world.

Notably, females carry a potential cure within their own cells. Every affected cell harbors a normal but dormant copy of *MECP2* on the inactive X (Xi) chromosome, which may, in principle, be reactivated to alleviate disease burden. Intriguingly, in male RTT mouse models, restoring normal *Mecp2* expression can reverse disease after the onset of symptoms (6, 7). There are, however, two obstacles to an Xi-reactivation strategy. First, sex chromosomal dosage compensation is known to be important throughout development and life: Perturbing XCI by a germline deletion of the master regulator *Xist* resulted in inviable female embryos (8), an epiblast-specific deletion of *Xist* caused severely reduced female fitness (9), and a conditional deletion of *Xist* in blood caused fully penetrant hematological cancers (10). Perturbing dosage balance via Xi reactivation could therefore have untoward physiological consequences. On the other hand, loss of Xist and partial reactivation occur naturally in lymphocytes (11), and may therefore be tolerated in vivo under controlled circumstances. A second challenge is that the Xi has been difficult to reactivate via pharmacological means due to multiple parallel mechanisms of epigenetic silencing (1–3, 12). Progress has been made in recent years, however. Several siRNA screens identified several factors regulating Xi stability, but no overlap of candidates was observed between them (13, 14), perhaps because the screens were not saturating. Others have identified the TGF-β pathway (15), a synergism between Aurora kinase and DNA methylation in a primed small-molecule screen (16), as well as a

Significance

The X-chromosome harbors hundreds of disease genes, a subset of which gives rise to neurodevelopmental disorders such as Rett syndrome (RTT), fragile X syndrome, and CDKL5 syndrome. There is presently no disease-specific treatment. Here, we work toward a therapeutic program based on reactivation of the silent X chromosome to restore expression of the missing protein. We develop a mixed modality approach that combines a small-molecule inhibitor of DNA methylation and an antisense oligonucleotide against Xist RNA. This combination achieves up to 30,000-fold methyl-CpG binding protein 2 upregulation in cultured cells. In vivo modeling using a conditional *Xist* knockout and 5-aza-2′-deoxycytidine recapitulates inactive X reactivation. These findings provide proof of concept for the mixed modality approach to treat X-linked disorders, including RTT.

Author contributions: L.L.G.C. and J.T.L. designed research; L.L.G.C. performed research; W.P., W.M., and R.J.K. contributed new mouse lines/analytic tools; L.L.G.C. and J.T.L. analyzed data; C.-Y. W. and C.W. performed bioinformatic analysis; and L.L.G.C. and J.T.L. wrote the paper.

Reviewers: I.B., UMass Medical School; and G.C., University of Michigan.

Conflict of interest statement: J.T.L. is a founder and scientific advisory board member of Translate Bio and Fulcrum Therapeutics. Patents have also been filed on the subject matter.

Published under the PNAS license.

Data deposition: The data reported in this paper have been deposited in the Gene Expression Omnibus (GEO) database, https://www.ncbi.nlm.nih.gov/geo (accession no. GSE97077).

[1]To whom correspondence should be addressed. Email: lee@molbio.mgh.harvard.edu.

This article contains supporting information online at www.pnas.org/lookup/suppl/doi:10.1073/pnas.1715124115/-/DCSupplemental.

synergism between a ribonucleotide reductase subunit (*RRM2*) and 5-aza-2′-deoxycytidine (17). In a more direct approach, an Xist RNA proteomic screen identified more than 100 interacting proteins and demonstrated that de-repression of the Xi could be achieved robustly only when two to three interactors were targeted simultaneously (18). In all studies to date, MECP2 restoration has been extremely limited (<<1% of normal levels). Here, we integrate the existing knowledge and explore new methods of Xi reactivation. We arrive at a mixed modality approach, including an antisense oligonucleotide (ASO) against Xist and an inhibitor of DNA methylation, the combination of which achieves a 30,000-fold reactivation of MECP2 from the Xi.

Results

Pharmacological Synergy Through a Mixed Modality Approach. While the pharmaceutical industry has focused almost exclusively on targeting proteins, long noncoding RNAs (lncRNAs) have become increasingly attractive as pharmacological targets (19). Improving ASO technology makes lncRNAs pharmacologically accessible. ASOs are high-molecular-weight compounds that have been optimized over the past 50 y through chemical modifications to acquire greater stability, selectivity, and bioavailability (20, 21). Since ASOs bind their target through Watson–Crick base-pairing interactions, they can be rationally designed and hit previously "undruggable" targets. Notably, ASO technology has achieved success in treating hypercholesterolemia (Kynamro) and spinal muscular atrophy (Spinraza).

We asked whether an ASO could also be developed for Xi reactivation and screened a small ASO library against various targets of potential interest, including Xist RNA and an antisense transcript to Mecp2 (Mecp2-as) (Fig. 1*A*, Fig. S1, and Table S1). In designing the ASOs, we chose phosphorothioate backbone and locked nucleic acid (LNA) chemistry (22) for its in vivo and in vitro stability, and increased affinity and selectivity for RNA targets. All were designed as gapmers, with unmodified deoxyribonucleotides in the center flanked by 5′ and 3′ terminal locked nucleotides, to direct RNase-H–mediated cleavage of the target transcript. We tested each ASO on an immortalized clonal mouse fibroblast cell line carrying an *Mecp2:luciferase* knock-in reporter on the Xi (15, 16). The luciferase reporter provides a highly sensitive enzymatic detection method with a large dynamic range. Because previous studies provide strong support for synergistic Xi reactivation (12, 16–18), we examined the efficacy of each ASO in the presence of 0.5 μM decitabine [5-aza-2′-deoxycytidine (Aza)] for 3 d. Notably, Aza combinations with ASOs against Mecp2-as or various nearby ASOs yielded inconsistent, low, or no Mecp2:luciferase reactivation relative to untreated samples or Aza-only samples. Remarkably, however, the Xist ASO + Aza combination showed a robust, reproducible response equivalent to 2% of normal MECP2 levels on the active X (Xa) (Fig. 1*B* and Fig. S1). These data suggest that targeting Xist RNA, together with DNA methylation, may be an effective method of achieving partial Xi reactivation.

Next, we performed the reciprocal analysis and asked whether combining the Xist ASO with small-molecule inhibitors of other epigenetic pathways may be efficacious. We tested commercially available compounds for factors identified in an Xist proteomic study (18) (Fig. 1*C* and Table S2). In combination with the Xist ASO, inhibitors of EZH2 (EPZ6438) and Aurora kinase (VX680) showed varying degrees of up-regulation (Fig. 1*D*). These inhibitors were previously identified as potential Xi reactivators in independent screens (13, 16). Intriguingly, none of the inhibitors against recently identified targets demonstrated an efficacy that rivaled Aza + Xist ASO (Fig. 1*D*), although we limited testing to Xist interactors for which small-molecule probes were available. Thus, in reciprocal tests of ASOs and small-molecule inhibitors, Xist ASO + Aza emerged as the top candidate. This mixed modality combination yielded a level of

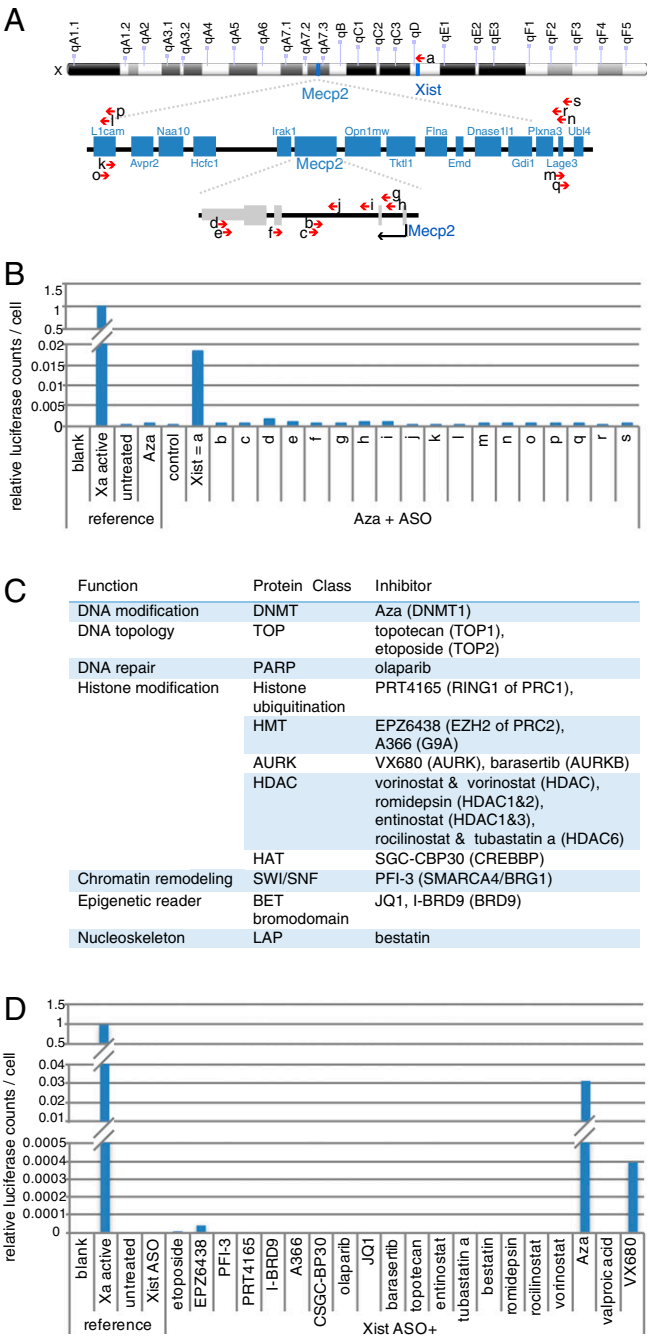


Fig. 1. Targeting the Xist interactome using a mixed modality approach. (*A*) Schematic representation of the directionality and locations of different tested ASOs on the X chromosome. (*B*) Luciferase assay results [corrected counts per second (CCPS)] normalized to the amount of cells of Xi-Mecp2-Luc MEFs treated with 20 nM ASO (lipofectamine transfection) and 0.5 μM Aza over 3 d. (*C*) List of the inhibitors tested and their protein targets. (*D*) Luciferase assay results (CCPS) normalized to cell number after treatment with different concentrations of small-molecule inhibitors (Table S2) and Xist ASO at 20 nM ASO (lipofectamine transfection) over 3 d.

reactivation not previously seen. Henceforth, we focus on characterization of this combination.

The Xist ASO + Aza Synergistic Duo. To exclude off-target effects, we created three Xist gapmers (1–3) that target different regions of exon 1 (Fig. 2*A*). Introduction of any single Xist ASO at 20 nM by lipofectamine transfection resulted in >95% Xist

depletion in mouse embryonic fibroblasts (MEFs) for 3–5 d (Fig. 2*B* and Fig. S2*A*). To test the Xist ASO + Aza combinations and look for potential Xi reactivation of *Mecp2*, we used the cell line carrying the *Mecp2:luciferase* reporter on the Xi. We examined five different Aza concentrations given as a single dose on day 0 against a fixed 20 nM concentration of the Xist (gapmer 1 was selected for further studies) or control [scrambled (Scr)] ASO and examined cells over a 3-d treatment period. Whereas Aza concentrations between 0 and 0.5 μM were tolerated, higher concentrations (1.0 and 2.5 μM) resulted in increased cell death (Fig. 2*C*). At 20 nM, the Xist ASO was not toxic relative to the control ASO (Fig. 2*C*, compare *Top Left* versus *Bottom Left*). These data suggest that the combination of 20 nM ASO and a single pulse of 0.5 μM Aza (its IC_{50}), would be well tolerated by MEF cells in culture. Notably, an Aza pulse was also used to prime cells in a small-molecule screen (16).

After 3 d of treatment (Fig. 2*D*, *Left*), neither the control Scr ASO (20 nM) nor Xist ASO (20 nM gapmer 1) resulted in measurable luminescent counts per second. Application of Aza (0.5 μM) by itself caused the previously reported baseline level of *Mecp2:luciferase* reactivation (13, 16, 17). On the other hand, combining this Xist ASO with Aza resulted in a significant synergistic increase, in accordance with the in vivo data. This level of increase was equivalent to 1.8% of the theoretical maximum (i.e., ~2% of the protein level of *Mecp2:luciferase* when it was carried on the expressed Xa). This is equivalent to a 12,000-fold increase in Xi-*Mecp2* expression and is considerably greater than the 600-fold up-regulation observed in a previous screen (16). When cells were treated for 5 d with the Xist ASO + Aza combination, *Mecp2:luciferase* up-regulation increased to as much as 2.0–3.5% (average of 2.5%, $n = 3$; Fig. 2*D*, *Right*) or up to 30,000-fold of Xi levels. Single treatments with the ASO or

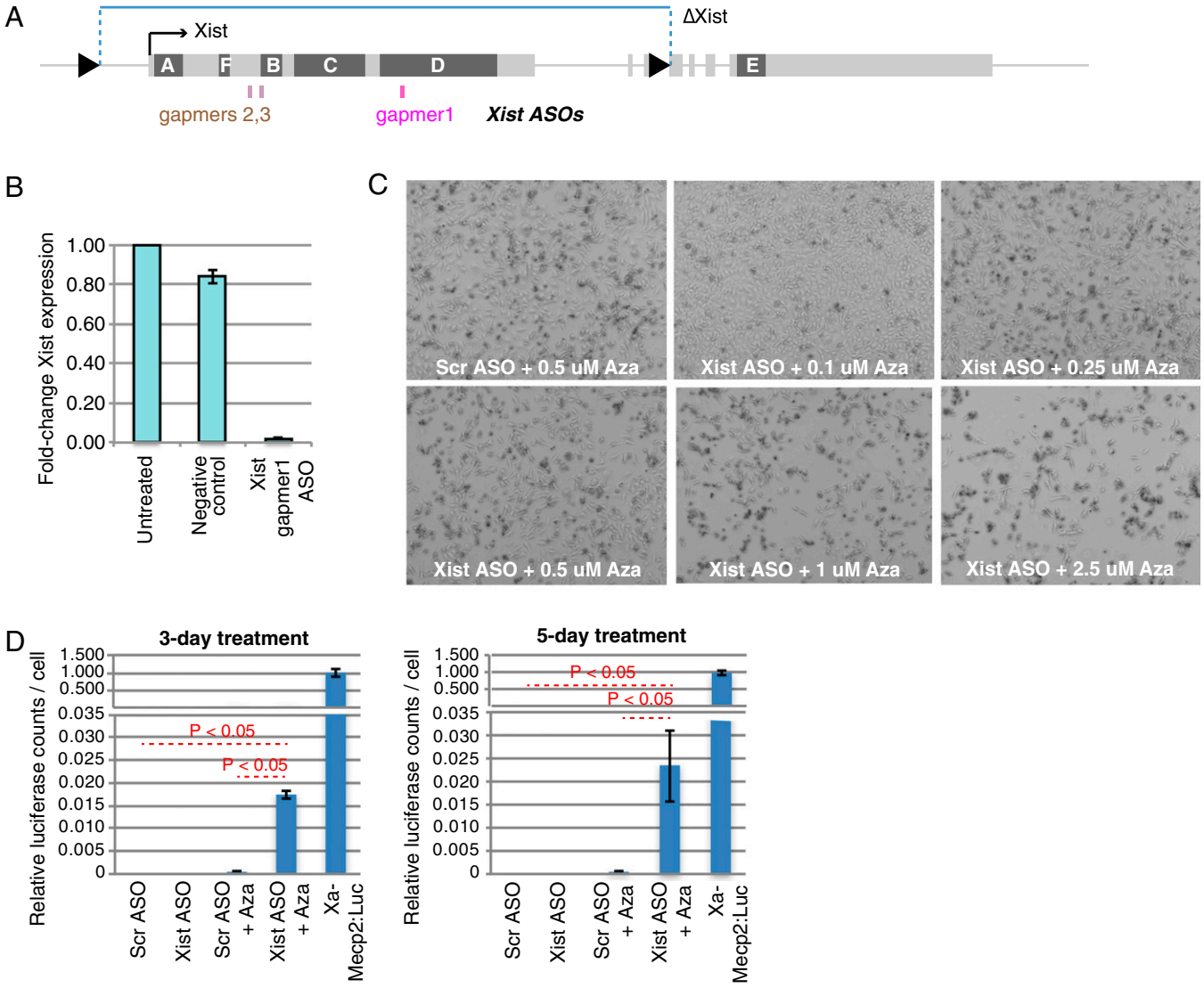


Fig. 2. Synergistic Xi reactivation by targeting Xist and DNA methylation in a cellular model. (*A*) Schematic representation of the *Xist* locus, with the *LoxP* sites of the conditional deletion allele (triangles) and regions targeted by Xist ASOs 1, 2, and 3. Conserved *Xist* repeat elements A–E are indicated. (*B*) qPCR results depicting the fold change in Xist RNA expression in cells treated with negative control ASO (Scr) and Xist ASO compared with untreated cells for 3 d ($n = 3$, replicates), normalized to Gapdh. Error bars represent SEM. (*C*) Bright-field microscope images at 4× magnification of Xi-Mecp2-Luc MEF cells treated with 20 nM Xist or control ASO, plus indicated concentrations of Aza. (*D*) Luciferase assay results of Xi-Mecp2-Luc MEFs treated with 20 nM Xist ASO and 0.5 μM Aza over 3 and 5 d. Results are scaled to the luciferase levels of the Xa-Mecp2-Luc clone (set at 1.0) ($n = 3$, replicates). Probability was determined by the Mann–Whitney *U* test (two-sided). Error bars represent SEM.

Aza remained significantly lower. To exclude off-target effects, two other Xist gapmers (gapmers 2 and 3; Fig. 2*A*) were tested and were also found to up-regulate MECP2 (Fig. S2 *B–D*).

Transcriptomic Analysis Indicates Selective Xi Reactivation. We asked if the Xist ASO + Aza combination achieved effects on the Xi beyond *Mecp2* reactivation. The Xi-reactivation strategy would have the potential to treat a number of X-linked diseases, including those caused by mutations of CDKL5, KIAA2022, USP9X, SMC1a, HDAC8, and FMR1. We tested the Xist ASO + Aza combination on a first generation (F1) hybrid fibroblast line in which the Xi is of *Mus musculus* (mus) strain origin and the Xa is of *Mus casteneus* (cas) strain origin (23). Between the X^{mus} and X^{cas}, there are over 600,000 X-linked sequence polymorphisms that enable determination of allelic origin (24). We established an allele-specific pipeline for RNA-sequencing (RNA-seq) analysis (Fig. 3*A*). Among 1,063 X-linked genes, only 510 were expressed [fragments per kilobase of transcript per million mapped reads (FPKM) > 0] in the fibroblast line. Among these, we considered only the 315 genes with a total number of allelic reads >12. Of these, 243 were considered to be subject to XCI, with a mus fraction of <1/11. RNA-seq analysis showed that $Xist^{cas}$ was not expressed from the Xa and that $Xist^{mus}$ expression from the Xi was knocked down by the ASO to nearly

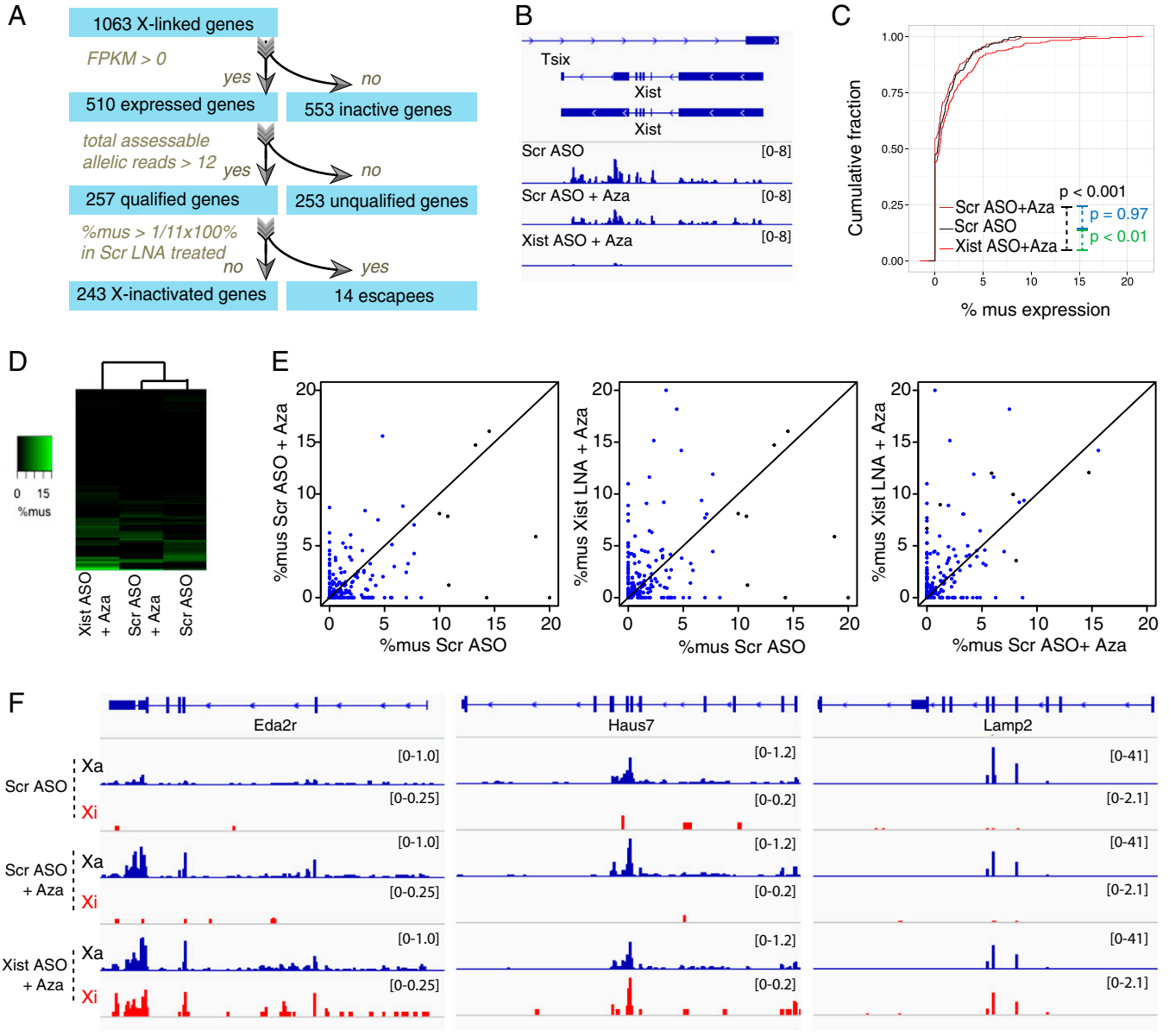


Fig. 3. Selective Xi reactivation using the Xist ASO + Aza combination. (*A*) Bioinformatic pipeline for allele-specific analysis of RNA-seq data. (*B*) RNA-seq traces of the Xi (mus) Xist expression in MEFs treated for 3 d with indicated drugs: ASOs were given at 20 nM, and Aza was given at 0.5 μM. The scales (brackets) are set to be equal across treatments. (*C*) CDP of the percentage of Xi expression, or [number of mus reads/number of (mus + cas)] reads × 100%, for MEF cells after each indicated 3-d treatment. Probability was determined by the Wilcoxon rank sum test (paired, one-sided). One biological replicate is shown. (*D*) Heat map of Xi (mus) expression of X-inactivated genes in each indicated sample, with hierarchical clustering. (*E*) Scatter plot of X-linked genes comparing the percentage of Xi expression ([number of mus reads/number of (mus + cas)] reads × 100%) in control (*x* axis) versus Aza- and/or Xist ASO-treated samples. (*F*) RNA-seq traces of reactivated genes in MEFs treated for 3 d with indicated drugs. ASOs were given at 20 nM, and Aza was given at 0.5 μM. Note the adjusted scales (brackets) set for Xi (mus: 0–0.25) or Xa (cas: 0–1) are shown within each gene.

undetectable levels (Fig. 3*B*). As a result, cumulative density plot (CDP) analysis of X-gene expression showed a significant right shift in Xi expression (allelic reads of Xi/Xi + Xa) when cells were treated with the Xist ASO + Aza combination in comparison to both the Scr ASO treatment and the Scr ASO + Aza treatment (Fig. 3*C*). Heat map (Fig. 3*D*) and scatter plot (Fig. 3*E*) analyses revealed a substantial number of Xi-reactivated genes in the Xist ASO + Aza-treated samples relative to treatment with Scr ASO and Aza. Specific genic examples also demonstrated the extent of Xi reactivation seen specifically in the combination treatment (Fig. 3*F*). RNA-seq did not offer enough sensitivity to see reactivation of *Mecp2*, especially in fibroblasts, where *Mecp2* is not expressed as highly as in neurons (*Mecp2* is not fused to luciferase in the hybrid cell line). Unlike the luciferase assay, a 2–5% increase in RNA-seq reads (FPKM) may be difficult to distinguish from noise. However, taken together, these data show a selective reactivation of the Xi relative to the Xa and the rest of the genome. They highlight the potential for treating other diseases and affirmed the idea of pharmacological synergy between depleting Xist RNA and treating with Aza.

Female Mice Lacking *Xist* in the Brain Live a Normal Life Span Without Reduced Fitness. In view of the reduced fitness of the mice lacking Xist RNA (9, 10), concerns might be raised for any treatment involving Xist depletion. Therefore, we next explored whether Xist loss and associated X-chromosome dosage change could be tolerated in the brain, the target organ of various X-linked neurodevelopmental disorders, including RTT, CDKL5 syndrome, and fragile X syndrome. Using a Nestin-Cre driver (25), we conditionally knocked out *Xist* in embryonic brain cells at embryonic day 11, a developmental stage long after establishment of XCI (Fig. 4*A*). Our cross resulted in heterozygous F1 females in whom *Xist* was deleted from the Xi in half of all neuronal cells. We then generated homozygously deleted F2 mice by backcrossing F1 *Xist*Δ/Y, Nestin-Cre male mice to female *Xist2lox/2lox* mice. We confirmed the deletions by RNA FISH and RT-qPCR for Xist expression. In F1 heterozygous females, the number of Xist RNA foci was reduced by half in the brain (Fig. S3 *A* and *B*), as were relative total Xist levels (Fig. 4*B*). In F2 homozygous females, Xist expression was absent in the brain (Fig. 4 *B* and *C*). In the liver, where Nestin-Cre was not expressed, Xist expression was unaltered.

We then asked whether brain-specific *Xist* deletion resulted in an overt phenotype in mice. In contrast to mice bearing *Xist* deletions in blood cells and the whole body (9, 10), both F1 and F2 *Xist*-mutant females were healthy and exhibited a life span similar to that of wild-type littermates (Fig. 4*D*). There was no difference in gait or mobility, as the mice showed equal performance on the rotarod (Fig. 4*E*). Some differences, such as in body weight, between mutant and wild-type mice were found, but these could be attributed exclusively to the Nestin-Cre knock-in (26) (Fig. S3 *C* and *D*). Notably, Nestin-Cre males, which should not be affected by an *Xist* deletion, nevertheless showed reduced size. The open-field and elevated plus maze tests also showed differences (Fig. S4). Because the cross as set up (Fig. 4*A*) rendered the Nestin-Cre allele and *Xist* deletions inseparable, the phenotype could be due to either the presence of Nestin-Cre (27) or the absence of *Xist*. Through an additional cross between an *Xist2lox*/$^{+}$ female and a Nestin-Cre male to separate the Nestin-Cre genotype from the *Xist2lox* genotype (Fig. S5), we attributed observed differences strictly to Nestin-Cre. Repeat open-field testing revealed the same significant differences between Xist2lox versus Nestin-Cre ($P < 0.02$), whereas the difference between XistΔ/$^{+}$ versus Nestin-Cre was insignificant ($P > 0.78$) (Fig. 4*F*). Because an intercross of F1 animals yielded F2 animals of nonuniform backgrounds, the F2 generation was not subjected to behavior testing.

Given minimal phenotypic differences, we performed RNA-seq analysis on the brains of F1 *Xist*Δ/$^{+}$ and F2 *Xist*Δ/Δ females at 1 y of age and looked for deviation of X-linked and autosomal gene expression relative to brains of *Xist2lox*/$^{+}$ and *Xist2lox/2lox* control females. Because the mice lacked allelic information that would allow distinguishing Xi from Xa expression, we analyzed composite (both alleles) gene activities on the X chromosome and displayed transcriptomic data in CDPs for fold changes between test and control brains (9) (Fig. 4*G* and Fig. S6*A*). Consistent with that observed in blood (10), loss of Xist resulted in up-regulation of X-linked genes relative to autosomes in two of three animals. Variability occurred between mice, as X up-regulation was not observed in animal 1. Thus, the Xi in the brain remains relatively stable despite deleting *Xist*. Reactivation, when it occurs, tends to be partial and variable in the brain.

Modeling Pharmacological Intervention in the *Xist*-Deleted Mouse. To assess whether Aza could synergize with the *Xist* deletion to destabilize the Xi in the brain, we treated *Xist*Δ/Δ female mice at 5 wk of age, the approximate age at which RTT phenotypes are clearly manifested. Cognizant of the cytotoxic effects of long-term Aza treatment (28), we tested short-term treatment on the principle that DNA methylation states are stably propagated, even through mitotic divisions (29, 30). Because Aza can cross the blood–brain barrier (31), we administered three sequential Aza pulses via i.p. injections over the course of 1 wk and then followed the health of these mice over time.

To examine changes in gene expression, we performed transcriptomic analysis on brain (target organ) and liver (control organ) harvested from a subset of mice at 2 wk after drug treatment. Three biological replicates were examined (Fig. 5 and Fig. S6). In the liver, where *Xist* was intact, X and autosomal gene expression remained balanced, even after triple-Aza treatment (Fig. 5*A* and Fig. S6*B*). Second, Aza treatment also did not result in X-to-autosomal gene imbalance in the *Xist2lox/2lox* brain (Fig. 5*A*). Three Aza pulses therefore did not result in global changes in X-linked or autosomal gene expression in *Xist*-positive tissues. Furthermore, deleting *Xist* alone had a minimal, variable effect on X-linked gene expression (Figs. 4*G* and 5*A*). On the other hand, combining the *Xist* deletion with pulse Aza treatment resulted in highly significant positive changes in X-linked gene expression relative to autosomal expression. Together, these data demonstrate that Aza treatment potentiates the effect of the *Xist* deletion in the brain, supporting a strong synergy between Xist and DNA methylation.

Notably, a short-term pulse treatment with Aza administered systemically (i.p.) was sufficient for Xist synergy across the blood–brain barrier over a 2-wk time frame. This is promising and suggests that Aza toxicity associated with long-term administration (28) could potentially be avoided. To determine if short-term treatment resulted in long-term toxicity, we followed treated animals over 1 y and noted no measurable differences in health and life span (Fig. 5*B*). Indeed, all mice have advanced to 1–2 y of age. At the time of treatment, the body weight of Xist2lox/2lox mice was, on average, higher than that of XistΔ/Δ mice, due to the Nestin-Cre background. Treatment did not introduce significant differences between weights of Aza- versus saline-treated mice (Fig. 5*C*). We conclude that short-term Aza treatment in *Xist*-deleted animals leads to a partial up-regulation of the X chromosome that is tolerated in vivo during the period of testing.

Discussion

The Xi is a reservoir of >1,000 functional genes that could, in principle, be tapped to treat disorders caused by mutations on the Xa. In the present study, we set out to define a pharmacological approach for selective Xi reactivation to restore expression

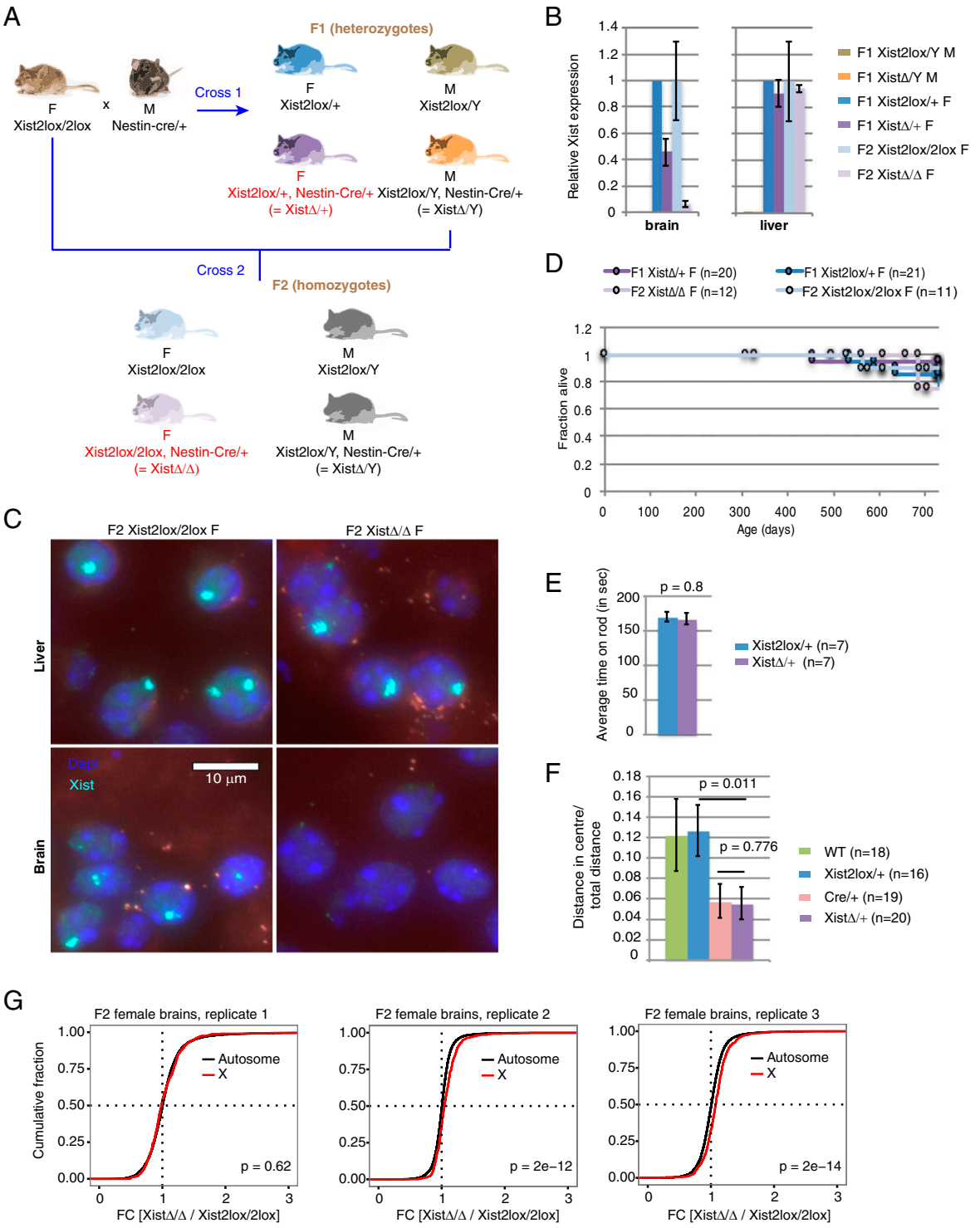


Fig. 4. Female mice with conditional deletion of *Xist* in the brain have a normal phenotype and life span. (*A*) Mating schemes to obtain F1 heterozygous and F2 homozygous female mice with brain-specific *Xist* deletion. F, female; M, male. (*B*) Relative Xist expression determined by qPCR in the brain and liver of F1 and F2 males and females, normalized to Gapdh ($n = 2$ mice). Error bars represent SEM. (*C*) Xist RNA FISH of brain and liver cells taken from indicated mice at the age of 530 d. Xist loss is evident in all cells of the *Xist*Δ/Δ brain (3% with one cloud, 97% with no cloud and 0% with two clouds, with $n = 367$ for F2 XistΔ/Δ brain F; 69% with one cloud, 30% with no cloud, and 1% with two clouds, with $n = 411$ for F2 XistΔ/Δ F liver; 75% with one cloud, 24% with no cloud, and 1% with two clouds, with $n = 280$ for F2 Xist2lox/2lox F brain; and 70% with one cloud, 19% with no cloud, and 11% with two clouds, with $n = 342$ for F2 Xist2lox/2lox F liver). A summary is also provided in Fig. S3*B*. (*D*) Kaplan–Meier survival curve shows normal life spans for all genotypes. (*E*) Summary of the rotarod analysis of 1-y-old female F1 mice with indicated genotypes and sample sizes. Probability was determined by a two-sided Student *t* test with equal variance. Error bars represent SEM. (*F*) Summary of the open-field test showing the ratio of the distance traveled in the center (measure of fear) to the total distance traveled (measure of activity) by 3-mo-old females of the four different genotypes. Differences were due to the Nestin-Cre, not to the *Xist* deletion (also Fig. S4 *A* and *B*). Probability was determined by a Mann–Whitney *U* test (two-sided). Error bars represent SEM. WT, wild type. (*G*) CDPs of fold change (FC) in X-linked (red curve) and autosomal (black curve) gene expression comparing F2 homozygous *Xist*Δ/Δ female brain with *Xist2lox*/2lox control in three sets of animals (at 91 and 7 wk). Probability was determined by the Wilcoxon rank sum test (unpaired, one-sided) ($n = 1$).

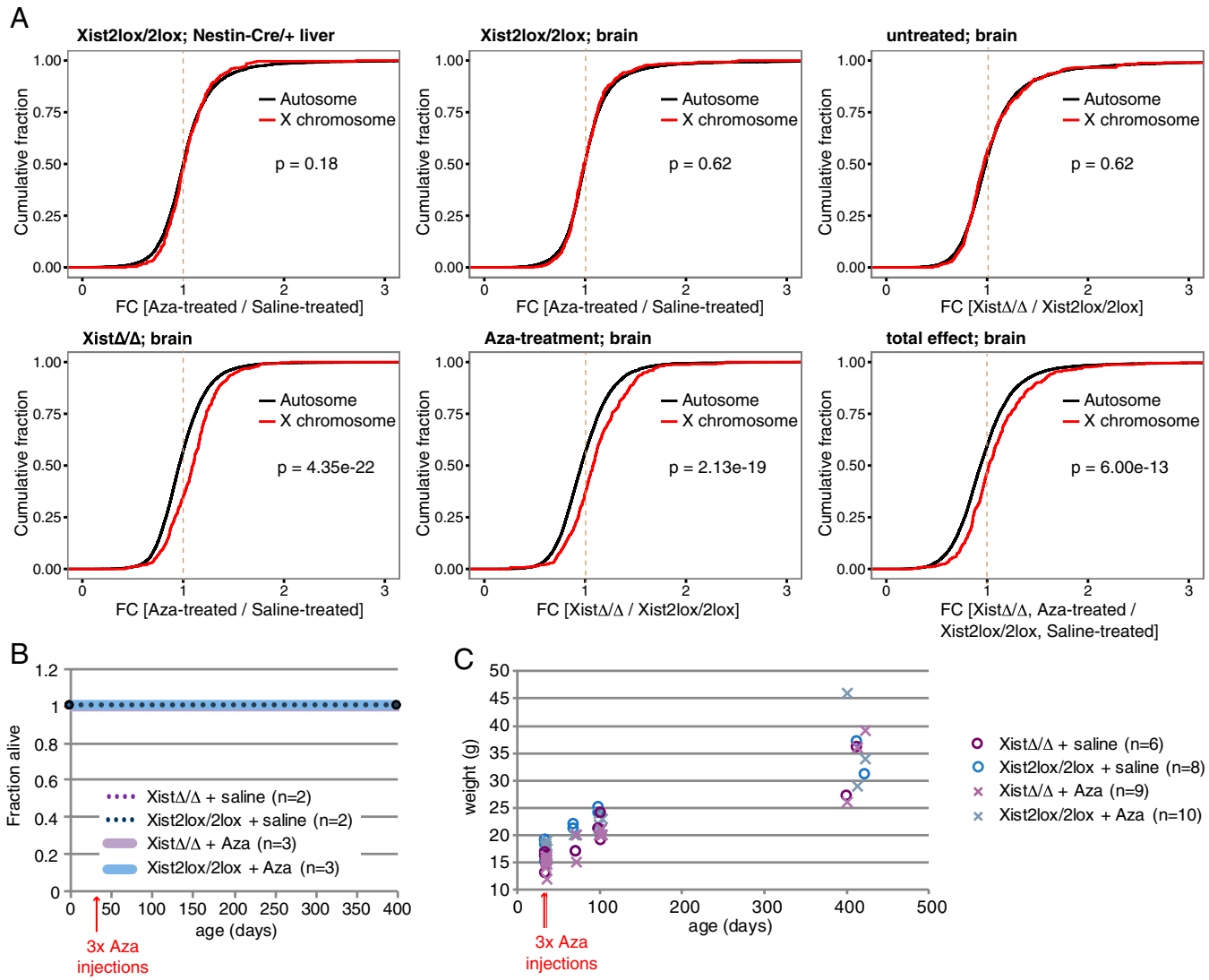


Fig. 5. Modeling synergistic Xi reactivation in a genetic model. Control and test mice underwent short-term Aza treatment. Aza was administered i.p. three times over 1 wk at the age of 5 wk. (*A*) CDPs of fold change (FC) in X-linked (red curve) and autosomal (black curve) gene expression comparing two samples as indicated. Probability was determined by the Wilcoxon rank sum test (unpaired, one-sided). Three replicates in total (also Fig. S6 *B* and *C*). (*B*) Kaplan–Meier curve of indicated mice. All mice are still alive as of this submission (circa 1 y of age). (*C*) Weight of indicated mice before and after treatment. All mice are represented at the point of injection and at 5 wk, 10 wk, or 1 y after injection (mice were divided into three groups). Statistically significant differences were found between mice with different genotypes but not between mice in different treatment groups, as determined by one-way ANOVA and Brown–Forsythe tests.

of missing X-linked gene products. We focused on RTT and restoration of MECP2, but our Xi-reactivation platform is agnostic to both the disease and the gene. Any gene residing on the X chromosome could be targeted in phenotypic, heterozygous females.

By targeting factors in the Xist interactome, we found that combining two drug modalities, a small molecule (Aza) + an ASO (Xist), achieved an unprecedented level of Xi reactivation and MECP2 protein up-regulation. The 2–5% up-regulation is equivalent to a 12,000- to 30,000-fold increase in Xi-*Mecp2* expression, is considerably greater than the 600-fold up-regulation observed in a previous screen (16), and thus marks significant progress for the Xi-reactivation platform. In vivo data have suggested that even 5% of normal *Mecp2* levels can have a profound impact on survival and overall function, as a previous report showed a slightly milder phenotype of *Mecp2-lox-stop-lox* male mice, due to their "leaky" termination cassette that enabled read-through *Mecp2* transcription (7). Thus, while the degree of up-regulation by the Xist + Aza combination did not exceed 5% in these experiments, this degree of restoration could have significant phenotypic consequences in vivo. Moreover, because our treatment period was brief (3–5 d) and the tolerable Aza concentrations in cell culture (0.5 μM; Fig. 2*C*) are still higher than concentrations typically used for mouse i.p. injections (32), in vivo outcomes may be enhanced by applying more concentrated doses. Our present analysis cannot distinguish between high-level MECP2 reactivation from a few cells versus low-level reactivation from a large percentage of cells. The two possibilities would have different physiological implications, but both are potentially relevant from a therapeutic standpoint, as MECP2 has been identified to have both cell-autonomous and non–cell-autonomous functions (33).

ASO drugs are generally more specific and have the advantage that information on pharmacokinetics and toxicity studies for chemically similar ASOs is transferable and cumulative. Thus, ASOs may have a more favorable path to regulatory approval.

Small molecules generally have lower selectivity and may face steeper hurdles in the approval process within the US Food and Drug Administration (FDA). By mixing modalities, our approach may potentially anticipate a more streamlined approach to FDA approval. We also note that Aza has already been approved by the FDA for other disease indications (myelodysplastic syndrome and acute myeloid leukemia) (34). Furthermore, our present in vivo data indicate that Aza need not be given continuously to have an impact on Xi reactivation in the brain, nor does Aza need to be injected into the target organ. Three short pulses delivered systemically were sufficient to induce Xi reactivation after 2 wk in the *Xist*-deleted brain. Unlike LNA-based ASOs, which have tissue half-lives of several weeks (22), Aza is known to have a very short half-life (<1 h in plasma) (35). However, once DNA is demethylated, the state may be stable (30). Future work will determine the duration of the effect and whether periodic Aza or ASO boosters might be necessary to maintain reactivation.

Finally, partial Xi reactivation in the brain does not cause apparent morbidity or mortality in the mouse. An important next step will be to test the drug in a RRT-specific disease model to look for phenotypic improvement. ASOs are well suited for the treatment of neurological diseases, and their delivery may be targeted to the central nervous system through intracerebroventricular or intrathecal injection (21), which has been considered acceptable and safe for serious disease such as ALS (36). Another critical next step will be the development of a better female mouse model that recapitulates the RTT disease severity (37) to test our Xi reactivation platform in vivo.

Materials and Methods

Animal procedures were approved by and performed in compliance with the Institutional Animal Care and Use Committee of Massachusetts General Hospital. Tissue culture, reactivation assays, mouse behavior analysis, and FISH were performed using standard procedures. A more detailed description of treatments and analysis is provided in *SI Materials and Methods*.

ACKNOWLEDGMENTS. We thank S. Sripathy and A. Bedalov for Mecp2-Luc cell lines, H. Sunwoo for FISH oligoprobes, and all other members of the J.T.L. laboratory for advice and feedback. L.L.G.C. was supported by the Belgian American Educational Foundation, the Platform for Education and Talent and Research Foundation - Flanders postdoctoral funding; R.J.K. was supported by the Simons Foundation Research Initiative; and J.T.L. was supported by the Rett Syndrome Research Trust and the NIH (Grant R01-DA36895). J.T.L. is an Investigator of the Howard Hughes Medical Institute.

1. Disteche CM (2012) Dosage compensation of the sex chromosomes. *Annu Rev Genet* 46:537–560.
2. Maduro C, de Hoon B, Gribnau J (2016) Fitting the puzzle pieces: The bigger picture of XCI. *Trends Biochem Sci* 41:138–147.
3. Lee JT (2011) Gracefully ageing at 50, X-chromosome inactivation becomes a paradigm for RNA and chromatin control. *Nat Rev Mol Cell Biol* 12:815–826.
4. Lyst MJ, Bird A (2015) Rett syndrome: A complex disorder with simple roots. *Nat Rev Genet* 16:261–275.
5. Katz DM, et al. (2016) Rett syndrome: Crossing the threshold to clinical translation. *Trends Neurosci* 39:100–113.
6. Giacometti E, Luikenhuis S, Beard C, Jaenisch R (2007) Partial rescue of MeCP2 deficiency by postnatal activation of MeCP2. *Proc Natl Acad Sci USA* 104: 1931–1936.
7. Guy J, Gan J, Selfridge J, Cobb S, Bird A (2007) Reversal of neurological defects in a mouse model of Rett syndrome. *Science* 315:1143–1147.
8. Marahrens Y, Panning B, Dausman J, Strauss W, Jaenisch R (1997) Xist-deficient mice are defective in dosage compensation but not spermatogenesis. *Genes Dev* 11: 156–166.
9. Yang L, Kirby JE, Sunwoo H, Lee JT (2016) Female mice lacking Xist RNA show partial dosage compensation and survive to term. *Genes Dev* 30:1747–1760.
10. Yildirim E, et al. (2013) Xist RNA is a potent suppressor of hematologic cancer in mice. *Cell* 152:727–742.
11. Wang J, et al. (2016) Unusual maintenance of X chromosome inactivation predisposes female lymphocytes for increased expression from the inactive X. *Proc Natl Acad Sci USA* 113:E2029–E2038.
12. Csankovszki G, Nagy A, Jaenisch R (2001) Synergism of Xist RNA, DNA methylation, and histone hypoacetylation in maintaining X chromosome inactivation. *J Cell Biol* 153:773–784.
13. Bhatnagar S, et al. (2014) Genetic and pharmacological reactivation of the mammalian inactive X chromosome. *Proc Natl Acad Sci USA* 111:12591–12598.
14. Chan KM, Zhang H, Malureanu L, van Deursen J, Zhang Z (2011) Diverse factors are involved in maintaining X chromosome inactivation. *Proc Natl Acad Sci USA* 108: 16699–16704.
15. Sripathy S, et al. (2017) Screen for reactivation of MeCP2 on the inactive X chromosome identifies the BMP/TGF-β superfamily as a regulator of XIST expression. *Proc Natl Acad Sci USA* 114:1619–1624.
16. Lessing D, et al. (2016) A high-throughput small molecule screen identifies synergism between DNA methylation and Aurora kinase pathways for X reactivation. *Proc Natl Acad Sci USA* 113:14366–14371.
17. Minkovsky A, et al. (2015) A high-throughput screen of inactive X chromosome reactivation identifies the enhancement of DNA demethylation by 5-aza-2′-dC upon inhibition of ribonucleotide reductase. *Epigenetics Chromatin* 8:42.
18. Minajigi A, et al. (2015) A comprehensive Xist interactome reveals cohesin repulsion and an RNA-directed chromosome conformation. *Science* 349:aab2276-1–aab2276-12.
19. Matsui M, Corey DR (2017) Non-coding RNAs as drug targets. *Nat Rev Drug Discov* 16: 167–179.
20. Bennett CF, Swayze EE (2010) RNA targeting therapeutics: Molecular mechanisms of antisense oligonucleotides as a therapeutic platform. *Annu Rev Pharmacol Toxicol* 50: 259–293.
21. Southwell AL, Skotte NH, Bennett CF, Hayden MR (2012) Antisense oligonucleotide therapeutics for inherited neurodegenerative diseases. *Trends Mol Med* 18:634–643.
22. Wahlestedt C, et al. (2000) Potent and nontoxic antisense oligonucleotides containing locked nucleic acids. *Proc Natl Acad Sci USA* 97:5633–5638.
23. Yildirim E, Sadreyev RI, Pinter SF, Lee JT (2011) X-chromosome hyperactivation in mammals via nonlinear relationships between chromatin states and transcription. *Nat Struct Mol Biol* 19:56–61.
24. Pinter SF, et al. (2012) Spreading of X chromosome inactivation via a hierarchy of defined Polycomb stations. *Genome Res* 22:1864–1876.
25. Tronche F, et al. (1999) Disruption of the glucocorticoid receptor gene in the nervous system results in reduced anxiety. *Nat Genet* 23:99–103.
26. Galichet C, Lovell-Badge R, Rizzoti K (2010) Nestin-Cre mice are affected by hypopituitarism, which is not due to significant activity of the transgene in the pituitary gland. *PLoS One* 5:e11443.
27. Giusti SA, et al. (2014) Behavioral phenotyping of Nestin-Cre mice: Implications for genetic mouse models of psychiatric disorders. *J Psychiatr Res* 55:87–95.
28. Momparler RL, et al. (1997) Pilot phase I-II study on 5-aza-2′-deoxycytidine (Decitabine) in patients with metastatic lung cancer. *Anticancer Drugs* 8:358–368.
29. Zaidi SK, et al. (2010) Architectural epigenetics: Mitotic retention of mammalian transcriptional regulatory information. *Mol Cell Biol* 30:4758–4766.
30. Kordasiewicz HB, et al. (2012) Sustained therapeutic reversal of Huntington's disease by transient repression of huntingtin synthesis. *Neuron* 74:1031–1044.
31. Chabot GG, Rivard GE, Momparler RL (1983) Plasma and cerebrospinal fluid pharmacokinetics of 5-Aza-2′-deoxycytidine in rabbits and dogs. *Cancer Res* 43:592–597.
32. Sales AJ, et al. (2011) Antidepressant-like effect induced by systemic and intrahippocampal administration of DNA methylation inhibitors. *Br J Pharmacol* 164: 1711–1721.
33. Kishi N, Macklis JD (2010) MeCP2 functions largely cell-autonomously, but also non-cell-autonomously, in neuronal maturation and dendritic arborization of cortical pyramidal neurons. *Exp Neurol* 222:51–58.
34. Welch JS, et al. (2016) TP53 and decitabine in acute myeloid leukemia and myelodysplastic syndromes. *N Engl J Med* 375:2023–2036.
35. Karahoca M, Momparler RL (2013) Pharmacokinetic and pharmacodynamic analysis of 5-aza-2′-deoxycytidine (decitabine) in the design of its dose-schedule for cancer therapy. *Clin Epigenetics* 5:3.
36. Miller TM, et al. (2013) An antisense oligonucleotide against SOD1 delivered intrathecally for patients with SOD1 familial amyotrophic lateral sclerosis: A phase 1, randomised, first-in-man study. *Lancet Neurol* 12:435–442.
37. Katz DM, et al. (2012) Preclinical research in Rett syndrome: Setting the foundation for translational success. *Dis Model Mech* 5:733–745.